frontiers | Frontiers in Materials

TYPE Original Research
PUBLISHED 17 May 2024
DOI 10.3389/fmats.2024.1374409

OPEN ACCESS

EDITED BY
Liqun Yang,
Shengjing Hospital of China Medical University, China

REVIEWED BY
Soodabeh Davaran,
Tabriz University of Medical Sciences, Iran
Guangqi Yan,
China Medical University, China

*CORRESPONDENCE
Yuanjun Xia,
yuanjunxia@aliyun.com
Ying Zhang,
zhangying_doc@aliyun.com

†These authors have contributed equally to this work

RECEIVED 22 January 2024
ACCEPTED 11 April 2024
PUBLISHED 17 May 2024

CITATION
Zhao L, Zhao X, Deng F, Ye X, Shen Z, Xia Y and Zhang Y (2024), Integration of BMP-2/PLGA microspheres with the 3D printed PLGA/$CaSO_4$ scaffold enhances bone regeneration.
Front. Mater. 11:1374409.
doi: 10.3389/fmats.2024.1374409

Integration of BMP-2/PLGA microspheres with the 3D printed PLGA/$CaSO_4$ scaffold enhances bone regeneration

Li Zhao[1†], Xiaoliang Zhao[1†], Fengpiao Deng[1†], Xiangling Ye[2,3], Zhen Shen[4], Yuanjun Xia[1,5]* and Ying Zhang[1,5]*

[1]Department of Orthopedics, General Hospital of Southern Commond Theater of PLA, Guangzhou, Guangdong, China, [2]Dongguan Hospital, Guangzhou University of Chinese Medicine, Dongguan, Guangdong, China, [3]The Second Clinical College of Guangzhou University of Chinese Medicine, Guangzhou, Guangdong, China, [4]Department of Rehablitaion, Kunming Municipal Hospital of Traditional Chinese Medicine, The Third Affiliated Hospital of Yunnan University of Chinese Medicine, Kunming, Yunnan, China, [5]The First School of Clinical Medicine, Southern Medical University, Guangzhou, Guangdong, China

Treatment of large and complex irregular bone defects is a major clinical challenge in orthopedic surgery. The current treatment includes bone transportation using the Ilizarov technique and bone cement repair using the Masquelet technique, but they require long-term manual intervention or secondary operation. To improve this situation, we compared the different implanting materials in the literature published in the past 10 years, finding that glycolic acid copolymer (PLGA) and Calcium sulfate ($CaSO_4$) are appropriated to be used as synthetic bone materials due to their advantages of easy-availability, nontoxicity, osteogenic properties and rapid degradation. Meanwhile, the development of 3D printing technique and devices makes it relatively easier to synthetize customized bio-mimetic porous scaffolds, thus facilitating the release of modified protein. In this study, we compounded BMP-2/PLGA microspheres with polylactic glycolic acid copolymer/$CaSO_4$ (PC) 3D printed scaffold to improve the osteogenic properties of the scaffold. The result of our *in vitro* experiment demonstrated that the prepared PCB scaffold not only had satisfactory bio-compatibility, but also promoted osteogenic differentiation. This 3D printed scaffold is capable to accelerate the repair of complex bone defects by promoting new bone formation, suggesting that it may prove to be a potential bone tissue engineering substitute.

KEYWORDS

bone defect, 3D printed, PLGA microspheres, calcium sulfate, BMP-2

1 Introduction

Bone defects are one of the most common clinical conditions and can be caused by trauma, tumors and skeletal abnormalities (Giannoudis et al., 2011). With the development and prevalence of transportation, the incidence of open fractures caused by high-energy injuries is increasing and becoming a serious health problem worldwide. Such injuries often cause complex bone defects, which pose a great challenge for clinical management (Myeroff and Archdeacon, 2011). Allogeneic bone transplantation, and artificial bone transplantation are among the other methods for the treatment of bone defects. However, the

shortcomings of bone transplantation limit its wider application; for instance, the current relatively single and fixed clinical bone graft substitutes are far from adequate for filling and repairing complex and variable bone defects (Dimitriou et al., 2011). Compared with simple internal fixation, bone transplantation usually takes months to complete numerous surgeries including installing and removing the bone material, or using an external fixator for the large bone defect, which often requires a relatively long rehab process, while the recovery of limb function may not be fully satisfied. As the currently available materials and techniques cannot meet all clinical requirements for large bone defects, there is an urgent need to search for a biomaterial that can meet the needs of various types of bone defects.

In recent years, three-dimensional (3D)-printed technology has received increasing attention in bone tissue engineering, knowing that it can obtain porous scaffolds with certain mechanical properties through precise parameter design (Kumar et al., 2011). Such scaffolds can not only meet a variety of bone defect filling requirements at the macroscopic level but also provide a good microenvironment for bone tissue regeneration and promote bone healing by simulating the natural human bone through precise parameter design (Lutzweiler et al., 2020). A variety of materials have been developed and used for 3D-printed scaffolds, including natural polymers (Liu et al., 2019; Farris et al., 2022), metals (Zadpoor, 2019; Ghorai et al., 2022), and ceramics (Ma et al., 2018; Eugen et al., 2023). However, limited by the materials themselves, the disadvantages of single-material scaffolds are also very obvious, such as the slow degradation of metal scaffolds or inadequate osteogenic induction (Helaehil et al., 2021). Therefore, researchers have focused on composite materials, hoping to solve the disadvantages of single materials through complementary advantages (Turnbull et al., 2018). PLGA is a biodegradable biopolymer approved by the US Food and Drug Administration (FDA) due to its good biocompatibility (Kumari et al., 2010), excellent processing properties (Lee et al., 2016), degradability and suitable mechanical strength. In addition, PLGA scaffolds can be loaded with various nanomaterials and a variety of bioactive factors to promote the regeneration of bone defects (Han et al., 2019). So, it is considered as one of the most promising materials for bone defect repair. In our previous study (Liu et al., 2022), we synthesized the PLGA/$CaSO_4$ scaffolds 3D-printed scaffolds (PC) with different ratios, and found that the incorporation of $CaSO_4$ with 20% wt in PLGA not only improved the mechanical properties of the scaffold but also enhanced its *in vitro* osteogenic effect (Liu et al., 2022), demonstrating that it is a promising material for bone repair. However, it is difficult to achieve sufficient bone defect repair with a single functional scaffold. Bone morphogenetic protein-2 (BMP-2) is a potent bone-inducing cytokine from the transforming growth factor-β (TGF-β) family and has currently been commonly used as a protein bone graft alternative (Chen et al., 2004). It is the most important and widely used bone growth factor because it promotes the early enrichment of osteogenic precursor cells at the site of bone injury, and their differentiation and mineralization into mature osteoblasts, thereby facilitating osteogenic repair (Zanotti et al., 2008; Kimura et al., 2010). However, it has the disadvantages of a short half-life, high price, and easy inactivation *in vivo* (Xu et al., 2019). Studies have shown that PLGA microspheres, as microcarriers for drugs or proteins, can protect the activity of proteins and achieve a slow release of proteins (Wei et al., 2006; Park et al., 2008).

In this study, we wrapped the BMP-2 into the PLGA to obtain microspheres and then composited them on the surface of PC scaffolds to prepare PCB scaffolds. Our experiment showed that the osteogenic ability of the PCB scaffolds was superior to that of the PC scaffolds *in vitro* (Figure 1). Therefore, PCB scaffolds may provide a new idea for the treatment of bone defects, especially large and complex defects.

2 Materials and methods

2.1 Scaffold preparation

2.1.1 Synthesis of 3D polylactic glycolic acid Copolymer/$CaSO_4$ scaffolds (PC)

The PLGA/$CaSO_4$ scaffolds were synthesized by using a biological 3D printer (Livprint® N series, Medprin, Guangzhou, China). PLGA and $CaSO_4$ (20 wt% of the quality of PLGA) powder were added into the beaker and then stirred evenly at 200°C. The mixture was then injected into the 3D printer and the scaffold was printed according to the set parameters of the previous study (Liu et al., 2022). The nozzle temperature was 180 °C, and the temperature of supporting substrates during FDM printing was 120 °C.

2.1.2 Synthesis of BMP-2/PLGA microspheres

BMP-2/PLGA microspheres were prepared using a double emulsion method (Li et al., 2022). 100 mg PLGA was dissolved in 2.5 mL dichloromethane (DCM, Macklin, China) and 0.2 mL BMP-2 solution (20 mg/mL) was added to the PLGA solution. The primary emulsion (W/O) was obtained after 30-se swirling, slowly dripped into 20 mL polyvinyl alcohol (PVA) solution (1% w/v), and swirled again for 2 min to form a double emulsion (W/O/W). The double emulsion solution was stirred at room temperature for 12 h in a fume cabinet to evaporate DCM. BMP-2/PLGA microspheres were collected by centrifugation (4,000 rpm, 5 min), washed with deionized water 3 times, and freeze-dried.

2.1.3 Synthesis of BMP-2/PLGA microspheres modified PLGA/$CaSO_4$ scaffolds (PCB)

Dopamine hydrochloride (2 mg/mL) and the PB scaffolds were added to the Tris buffer solution (pH = 8.5). After being stirred for 48 h, they were taken out and placed in a dehumidifier to dry. Then, these scaffolds were placed into PLGA microspheres solution (4 mg/mL) and mixed in a decolorization shaker for 4 h. Finally, the scaffolds were dried in a dehumidifier and PCB scaffolds.

2.2 Characterization of scaffolds

2.2.1 Scanning electron microscopy (SEM) analysis

The surface morphology and pore size of the scaffolds were evaluated by SEM. All samples were dried under vacuum, coated with gold, and then the sample placed on the sample stage of

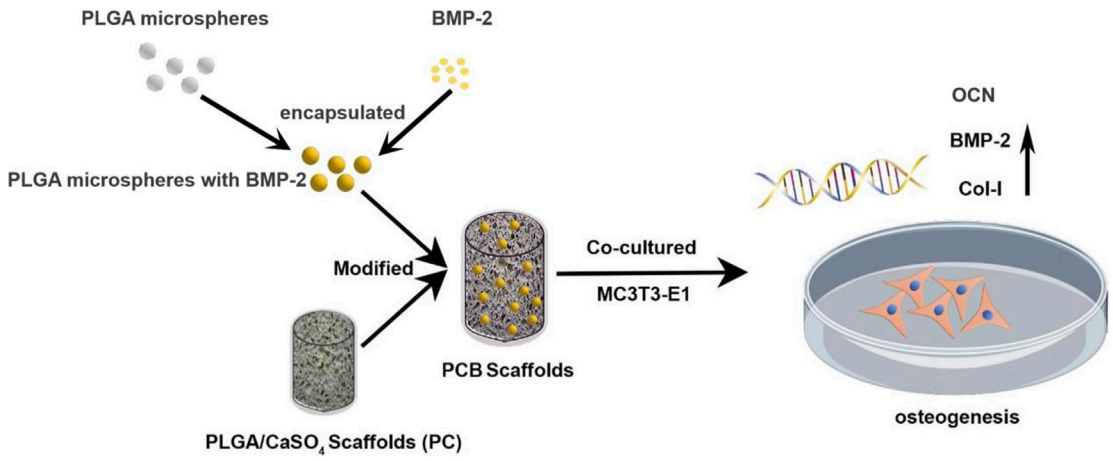

FIGURE 1
Schematic illustration of the preparation of scaffolds and osteogenesis *in vitro*.

SEM, using SEM (EM-30, COXEM, South Korea) to observe the structure, surface, and compression fracture morphology of the samples.

2.2.2 X-ray diffractometer (XRD) analysis

X-ray diffraction (DMX-220, Rigaku, Tokyo, Japan) was performed to investigate the scaffolds using Cu Kα X-rays generated at 40 kV and 30 mA at a diffraction angle (2θ) from 10° to 60° with a step size of 0.05°/step and an interval of 0.2 s/step.

2.2.3 Contact angle

The hydrophilicity of each scaffold was measured using a contact angle measurement system (ASUMI GIKEN Limited, Tokyo, Japan). A droplet of deionized water was deposited on the scaffold. Then, the image of the static liquid deposition was obtained within a few seconds and the contact angles were measured. Three samples were assessed for each group to ensure reproducibility and the average value.

2.2.4 Encapsulation efficiency of BMP-2/PLGA microspheres and *in vitro* release kinetics of PCB scaffolds

10 mg BMP-2/PLGA microspheres were added to a mixture of 0.9 mL NaOH (1 mol/L) and 0.1 mL PBS, shaken at room temperature for 2 h, and neutralized by addition of 1 mL 0.9 mol/L HCl. The BMP-2 concentration in the solution was detected using a human BMP-2 ELISA kit (Abcam) according to the manufacturer's instructions. The encapsulation efficiency was calculated using the following formula (1):

$$\text{Encapsulation efficiency} = \text{Actual protein loading} / \text{theoretical protein loading} \times 100\% \quad (1)$$

Subsequently, the sustained release of BMP-2 was measured as follows: 10 mg BMP-2/PLGA microspheres coated on the PCB scaffold were soaked in 2 mL PBS and incubated at 37°C and 100 rpm. At the set time intervals, 1 mL supernatant was collected by centrifugation and the BMP-2 content in the supernatant was determined using the human BMP-2 ELISA kit. 1 mL fresh PBS was added every time after the supernatant was collected.

2.2.5 Degradation of scaffolds

The degradation and pH values of the scaffolds were investigated over 6 weeks in simulated body fluid (SBF). Initially, the scaffolds were weighed (m1) and subsequently immersed in centrifuge tubes containing 10 mL SBF at 37°C. After rinsing the scaffolds with distilled water, they were dried until reaching a stable weight and then re-weighed (m2) over 6 weeks. The degradation rate was calculated using the formula: (m1−m2)/m1×100%. The pH of the degradation medium was measured using a pH meter from Mettler Toledo.

2.3 *In vitro* study

2.3.1 Cell proliferation and biocompatibility

Cell Counting Kit-8 (CCK-8) was used to assess the proliferation of MC3T3-E1 cells co-culture with the sterile scaffolds. 1 mL suspension of cells (1×10^4/mL) was seeded in 24-well plates in different scaffolds and incubated. After co-culture for 1, 3, and 5 days, 500 μL CCK-8 solution (10%) was added to each well for continuous incubation for 1 h. Then, optical density (OD) was measured at 450 nm using a microplate reader (Multiskan GO, Thermo Scientific, USA).

2.3.2 Live/dead staining

The cytotoxicity of scaffolds was also determined by live/dead staining classically. MC3T3-E1 cells were co-cultured with scaffolds as described above. On days 1, 3, and 5, each well was washed with PBS gently after removing the medium, and stained with 1 μM calcein-AM (Beyotime Biotechnology, China) and 2 μM propidium iodine (PI) for 30 min. The stained samples were then analyzed using a fluorescence microscope (Leica, Germany).

2.3.3 Hemolysis test

Healthy human blood was collected in anti-coagulant tubes and then 8 mL of blood was taken and diluted with around 10 mL of PBS. Then 0.2 mL of this diluted blood was added to 5 mL of PBS and further scaffolds were added. PBS and deionized (DI) water added of 0.2 mL were set as the negative and positive control. Then these test samples along with controls were incubated at 37°C for 30 min and centrifuged at 3,000 rpm for 10 min. The supernatant was collected and its optical density (OD) was measured at 545 nm. The hemolysis ratio (HR) was calculated as follows:

$$HR(\%) = \left(OD_{sample} - OD_{negative\ control}\right) / \left(OD_{positive\ control} - OD_{negative\ control}\right) \times 100$$

2.3.4 Alkaline phosphatase (ALP) staining

For ALP staining, MC3T3-E1 cells were seeded in a 6-well plate at a density of 1×10^4 cells per well and incubated with different scaffolds for 7 days. ALP activity was assayed using the BCIP/NBT alkaline phosphatase color development kit (Beyotime, China) according to the manufacturer's instructions. After removing the ALP stain working solution and washing with PBS, the stained MC3T3-E1 cells were visualized with an inverted research microscope (Leica, Germany).

2.3.5 Alizarin red S staining (ARS)

After 14 days culture as described above, the medium was removed and the cells were washed with PBS 3 times, fixed with 4% paraformaldehyde for 30 min, washed twice with double-distilled water (ddH_2O), and stained with ARS solution (Solarbio, China) for 2 h. After removing the dye solution and washed with ddH2O three times, cells were observed under a microscope (KEYENCE, VK-X1,100, Tokyo, Japan). To quantitatively evaluate the coloration, 10% cetylpyridinium chloride solution was added to each scaffold and incubated for 2 h. The solution was transferred to an Eppendorf tube and centrifuged at 13,000 rpm for 15 min. From each group, 100 μL solution was collected, placed in a 96-well plate, and measured using a microplate reader at 620 nm.

2.3.6 Expression of osteogenic genes

The osteogenic gene expression level of MC3T3-E1 was evaluated by real-time quantitative polymerase chain reaction (RT-qPCR). After 7 and 14 days of culture, total RNA was extracted using TRIzol reagent (AG, China), and then reverse transcribed into cDNA using a reverse transcription kit (AG, China). The gene expression of osteogenesis-related factors BMP-2, COL-1, and OCN was quantitatively detected using SYBR Green qPCR kit (AG, China), using the housekeeper gene GAPDH as a control. The primer sequences for all genes are listed in Supplementary Table S1.

2.3.7 Immunofluorescence (IF) staining

The expression of BMP-2 was further evaluated by IF staining. Briefly, after 14 days of culture, MC3T3-E1 was fixed with 4% paraformaldehyde, washed with PBS 5 times, and blocked with 5 wt% BSA in PBS at 37 °C for 30 min. After adding 200 μL rabbit anti-Rat BMP-2 IgG antibody (Abcam, UK, diluted 1:200 in PBS), samples were incubated at 37 °C for 12h, washed with PBS again 5 times, added with 200 μL goat anti-rabbit IgG antibody (Abcam, UK, diluted 1:500 in PBS), and incubated at 37 °C for 1 h. After five washes with PBS, the nucleus was stained with 4,6-diamino-2-phenyl indole (DAPI) for 5 min at room temperature. Finally, the stained cells on the samples were observed using an inverted fluorescence microscope (Nikon, Japan).

2.4 Statistical analysis

The analysis was performed by SPSS (V20. IBM Corp). The experimental results are expressed as the mean ± standard deviation (SD). The significance level was determined by an analysis of variance. Statistical significance was set at $p < 0.05$.

3 Results and discussion

3.1 Synthesis and characterization of scaffolds

PLGA microspheres are often used as microcarriers for drugs or proteins to protect the activity of proteins and achieve slow release of proteins (Wei et al., 2006; Park et al., 2008). In this study, we used a strategy of PLGA microspheres encapsulating BMP-2 to achieve a long-lasting slow release of bone morphogenetic protein (BMP-2) to better promote bone defect repair. It was found that the BMP-2/PLGA microspheres were spherically shaped with a smooth and rounded surface and a mean particle size of approximately 182 ± 54.68 nm, with 72.18% of the microspheres ranging from 150–220 μm in size (Figure 2A). The encapsulation rate of the BMP-2 microspheres was 48.55% ± 5.67%. Subsequently, we used the classical method to synthesize the PC 3D-printed scaffolds (Ye et al., 2022). As reported in our preliminary study (Liu et al., 2022), the PC scaffold was a typical plastic material, and its stress-strain was improved markedly compared with the pure PLGA material. When the content of $CaSO_4$ was 20%wt, it is breaking strength and yield strength reached the maximum, with the best compressive strength and shore hardness, close to the natural cancellous bone, which is a more ideal scaffold material for bone tissue engineering. To further improve the osteogenic effect of the scaffolds, we compounded BMP-2/PLGA microspheres on the PC scaffolds. The electron micrographs of PC and PCB scaffolds are shown in Figure 2B. It could be found that all scaffolds had a regular 3D porous structure, which facilitates the growth of osteoblasts and blood vessels (Swanson et al., 2021). In particular, when the BMP-2/PLGA microspheres were compounded with PC scaffolds, the scaffold surface became rougher, which was more favorable to the adhesion of osteoblasts (Chen et al., 2018; Rahmati et al., 2020).

The XRD patterns (Figure 2C) of the PC scaffolds showed characteristic crystalline peaks at 15, 25, 30, 31, and 48° corresponding to (200), (020), (002), (102), and (302) planes of $CaSO_4$ (Sindhura Reddy et al., 2014; Zhu et al., 2022), indicating the successful doping of the CaSO4 into the PC scaffolds. However, when the BMP-2/PLGA microspheres were compounded with the scaffolds, all the characteristic absorption peaks of $CaSO_4$ disappeared, indicating that the microspheres were successfully

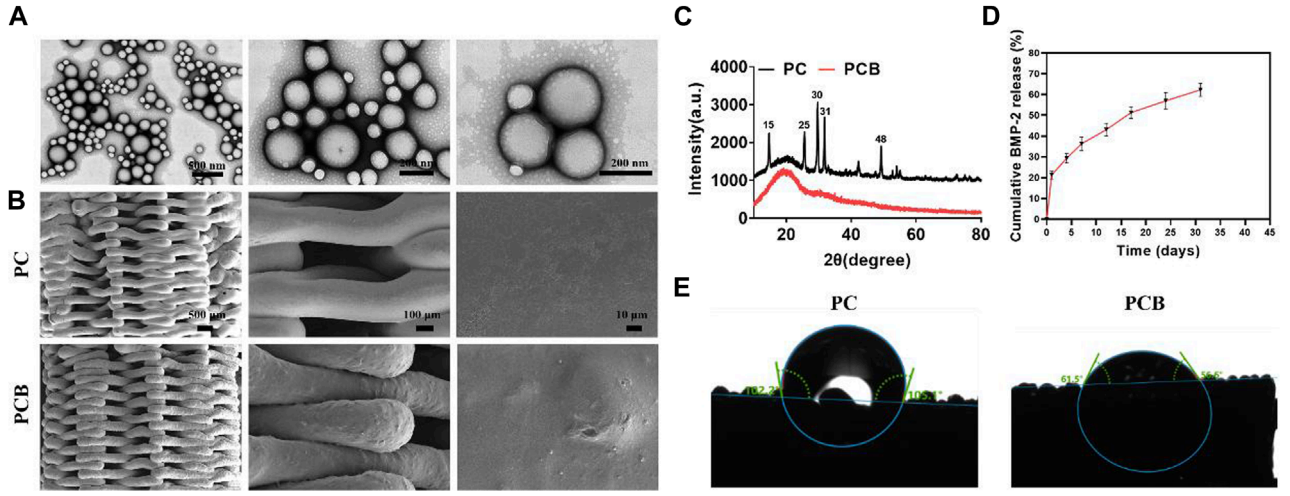

FIGURE 2
Characterization of scaffolds. **(A)** SEM images of the BMP-2/PLGA microspheres. **(B)** SEM images of the scaffolds. **(C)** XRD analysis of the scaffolds. **(D)** Release kinetics of the PCB scaffolds *in vitro*. **(E)** Contact angle measurement of the scaffolds.

coated on the printed filament surface of the PC scaffolds, resulting in a weakened signal for detection. The surface hydrophilicity of the scaffolds was evaluated by the water contact angle test. The encapsulation rate of the BMP-2 microspheres prepared in this study was tested as 67.13% ± 9.43%. The release profile of BMP-2 from the PCB scaffolds *in vitro* is shown in Figure 2D. The release of BMP-2 on the first day was approximately 21.36% and the subsequent release rate gradually slowed down to approximately 58.92% ± 3.14% by day 30. It was found that with the degradation of PLGA, BMP-2 was still slowly released after more than 30 days, thus effectively and continuously promoting osteogenic differentiation. The contact angle images of the scaffolds are shown in Figure 2E. It was found that the addition of BMP-2/PLGA microspheres reduced the contact angle of the scaffold and therefore the PCB scaffold was more hydrophilic, knowing that hydrophilicity plays an important role in protein uptake and cell proliferation (Liu et al., 2018).

The degradation performance of materials holds significant importance in bone tissue engineering. The degradation products of materials should be non-toxic to surrounding tissues and not induce allergic reactions or rejection. Excellent degradation performance ensures that the material can harmoniously coexist with biological tissues in the body. The degradation rate of materials should match the rate of new tissue formation. If the degradation rate is too slow, the implant may persist for an extended period, affecting the development of new tissues. Conversely, if the degradation rate is too fast, the material may lose its function before new tissue formation occurs. We found that the scaffolds degraded slowly in the first 2 weeks (Figure 3A). The early and slow degradation of the scaffold can provide long-term stable support after implantation, which is crucial for initial bone tissue formation. The existence of the scaffold can simulate the structure of natural bone and provide support during the process of bone cell adhesion, proliferation, and differentiation. In addition, the slow early degradation of the scaffold can also allow new bone tissue to grow on its surface, while the mechanical properties of the scaffold gradually weaken. This smooth transition helps avoid stress concentrations and promotes adaptive growth of the new bone tissue. After 2 weeks, the degradation rate of the scaffold accelerated and was degraded at 6 weeks. As shown in Figure 3B, after 6 weeks of soaking in SBF solution, the pH value of the scaffold showed a slowly decreasing trend, and there was no significant difference in the change of culture medium pH during degradation.

3.2 *In vitro* biocompatibility of the scaffolds

Biocompatibility is one of the most important functions of biomaterials, which requires that the materials have no damage to cells and tissues (Wang et al., 2020). In our previous study, we used the CCK-8 assay to test the cytotoxicity and proliferation of the scaffolds, finding that PC scaffolds had good biocompatibility *in vitro* (Liu et al., 2022). First, we verified the biocompatibility of the scaffolds again using live/dead cell staining (Figure 4A). The number and proportion of live cells (green) and dead cells (red) were similar in both PC and PCB scaffold groups compared with the control group. Then, we further explored the effect of the scaffolds on cell proliferation in the two groups (Figures 4B, C) and found that after co-culturing the MC3TE-E1 cells with scaffolds for 1, 3 and 5 days, cell proliferation was the same in each group, indicating that none scaffold had significant adverse effects on cell proliferation, which is consistent with the results of live/dead cell staining experiment. These results show that our scaffolds have good biocompatibility *in vitro* and can meet the basic requirements for bone tissue engineering scaffolds. The hemolysis test is another essential parameter to assess the safety of biological materials, reflecting the rejection of the implant by the blood in the body (Wang et al., 2019). As shown in Figure 4D, the supernatant of the positive control group was red due to the rupture of erythrocytes in response to hemolysis. In contrast, the supernatant of the other two groups of stents and the negative control group was

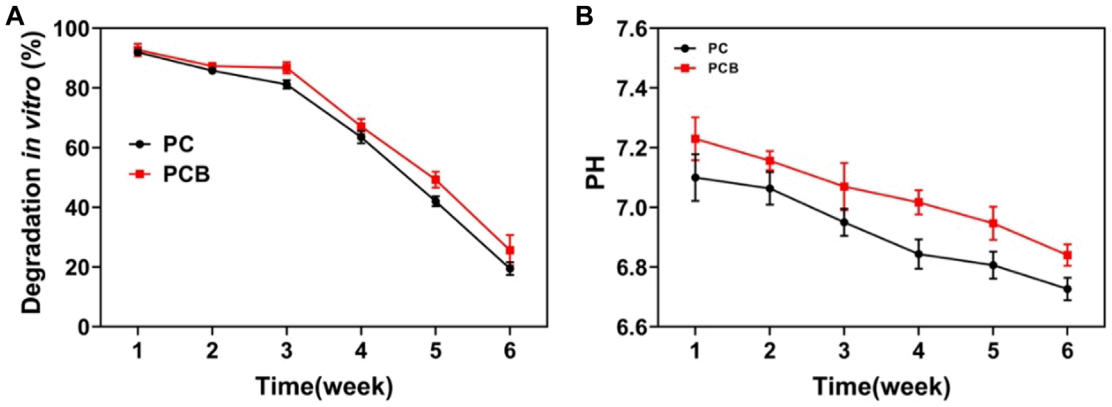

FIGURE 3
Degradation of the scaffold. **(A)** Weight of scaffolds after degradation *in vitro*. **(B)** pH value in the simulated body fluid.

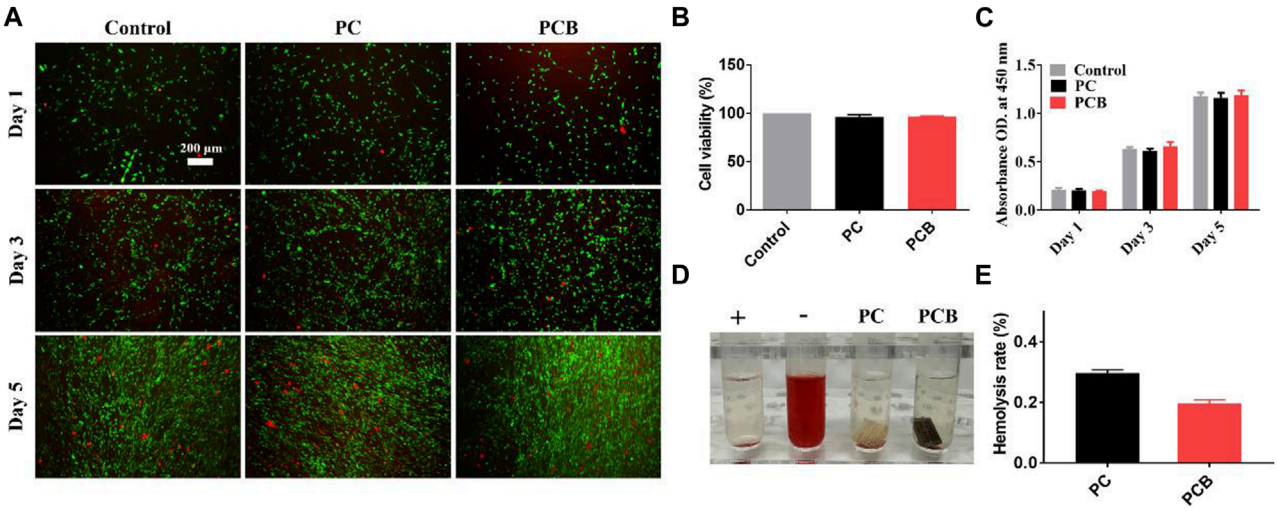

FIGURE 4
Biocompatibility of the scaffolds *in vitro*. **(A)** Live/dead staining of preosteoblasts after incubation with the scaffolds. Scale bar = 200 μm. **(B)** Cell viability of preosteoblasts after incubation with scaffolds. **(C)** The proliferation of preosteoblasts after 1, 3, and 5 days of incubation with the scaffolds (determined by a CCK-8 assay). **(D)** Hemocompatibility test and hemolysis rate of the scaffolds. **(E)** The hemolysis ratio was measured at 545 nm. Data are presented as the mean ± SD ($*p < 0.05$, $**p < 0.01$, $***p < 0.001$; $n = 3$).

a clarified solution, and the hemolysis rate was less than 0.5% (Figure 4E), proving that all stents had a negligible effect on erythrocytes.

3.3 *In vitro* osteoinductivity of the scaffolds

Bone tissue engineering scaffolds should have good osteoconductivity and osteoinductivity to facilitate the repair of bone defects (Tang et al., 2016). Among them, osteoinductivity refers to its ability to contribute to osteogenic differentiation and is an important index for the performance evaluation of bone repair materials (Meijer et al., 2007). In this study, we used ALP staining, alizarin red staining, cellular IF analysis, and osteogenesis-related gene expression levels to detect the *in vitro* osteoinductivity of the scaffolds. ALP is an exonuclease of osteoblasts, and its expression activity is an important marker of osteogenic differentiation (Sun et al., 2018). Figure 5A shows ALP staining of MC3T3-E1 cells after 7-day co-culture, demonstrating that ALP staining in the PC scaffold group was not significantly deeper than that in the control group, both were lavender in color, and a small number of calcium crystals are visible in the field of view. However, the staining of the PCB scaffold group was significantly deeper, with a dark purple color, and a large distribution of calcium crystals could be seen microscopically. This result suggests that the released BMP-2 protein significantly promoted the osteogenic differentiation of MC3T3-E1 as the microspheres were compounded.

10.3389/fmats.2024.1374409

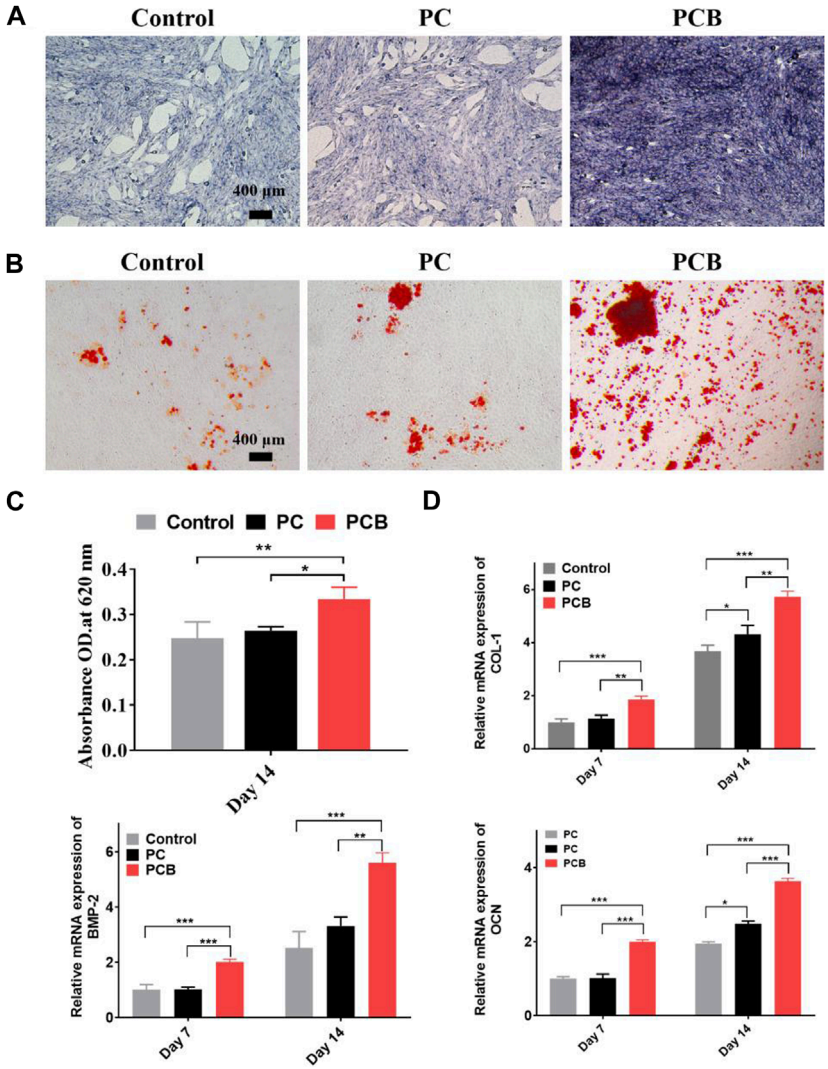

FIGURE 5
In vitro osteogenesis of the scaffolds. **(A)** ALP staining of preosteoblasts after 7-day culture with the scaffolds. Scale bar = 400 μm. **(B)** Alizarin red S staining of the extracellular calcium nodules in preosteoblasts cultured with the scaffolds for 14 days. Scale bar = 400 μm. **(C)** Semi-quantitative analysis of alizarin red S staining. Cetylpyridinium chloride solution. The stained extracellular calcium nodules were dissolved in a cetylpyridinium chloride solution. **(D)** The relative expression of ontogenetic genes of preosteoblasts cultured with different scaffolds. **(E)** Representative images of IF staining of BMP-2. Data are presented as the mean ± SD ($*p < 0.05$, $**p < 0.01$, $***p < 0.001$; $n = 3$).

Calcium nodules are a product of late osteogenic differentiation, which can be detected by binding specifically to an alizarin red stain to form a dark red substance (Lee et al., 2020). The result of alizarin red staining of each scaffold group showed that the number of calcium nodules in the PCB scaffold groups was significantly increased compared with the scattered calcium nodules in the control group and PC group (Figure 5B). Microscopically, MC3T3-E1 cells produced a large number of calcium crystals after the addition of BMP-2/PLGA microspheres, which gradually fused into clusters and were deeply stained by the staining solution, indicating that the osteogenic differentiation of cells in the PCB group was more advanced. Semi-quantitative analysis showed that OD in both PC and PCB groups was higher than that in the control group, being the highest in the PCB group (Figure 5C). These data demonstrate that PT/CA/Cu scaffolds possess excellent osteoinductivity.

The expression levels of osteogenic-related genes also directly reflect the level of osteogenic differentiation of cells. We examined the expression levels of BMP-2, COL-1, and OCN genes using qt-PCR, and the results are shown in Figure 5D. The mRNA expression levels of all three genes showed similar trends, with the highest expression in the PCB group, followed by the PC group, and the lowest expression in the control group. Gene expression levels in the PC group were only upregulated at day 14 except for the BMP-2 gene, which might be related to the release of more calcium from scaffold degradation. In contrast, the expression of the remaining PCB groups was significantly higher at both 7 and 14 days compared with the control group, demonstrating a stronger osteogenic effect. It is interesting to find that the BMP-2 gene was most upregulated in the PCB group at day 14 compared with COL-1. COL-1 expresses the type I collagen, which is a major component of the extracellular

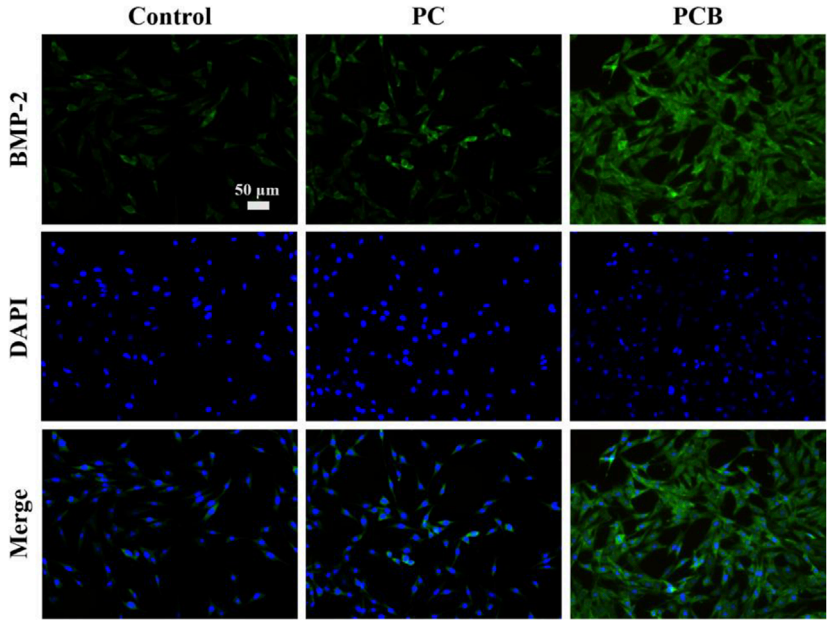

FIGURE 6
Representative images of immunofluorescence staining of BMP-2. Scale bar = 50 μm.

matrix and could direct calcium salt deposition and mineralization, thus promoting new bone formation (Park et al., 2014). This would also explain why the difference in our ALP staining was significantly higher than the result of the alizarin red staining.

Based on the above results, we used cellular IF to further detect the protein expression level of the BMP-2 gene, and the results are shown in Figure 6. After 14-day co-culture, the expression level of BMP-2 was generally low and the fluorescence signal was weak in the control groups. However, we found that the fluorescence signal was enhanced in the other two groups, and the PCB group had the highest fluorescence intensity, which was significantly different from the rest of the scaffolds. This indicates that the osteogenic differentiation of the cells gradually deepened as the osteogenic induction proceeded, and the effect was more obvious with the addition of BMP-2/PLGA microspheres, which is consistent with the previous findings. In summary, our study shows that PCB scaffolds can effectively promote the osteogenic differentiation of cells and are expected to accelerate the repair of bone defects.

Repairing bone defects by using artificial bone material has been widely researched in recent years, and its most essential property is its osteogenic ability. With the development of nanometer materials and 3D printing, many innovative materials were designed and proved their effectiveness. Some researchers have summarized the application of nanofiber scaffolds in hyaline cartilage tissue repair (Ahmadian et al., 2023). Due to the natural association between bone cells and highly nano-rough surfaces, the adhesion ability and biocompatibility of nano-modified scaffolds are effectively improved. Besides, by using internal and external triggers, the release of growth factors and cells could be more precisely and individually controlled (Khalilov, 2023). Therefore, we can also expect the application of nanometer materials in the research about complex bone defects/infections by precisely and individually designing the modified growth factor or antibiotics.

4 Conclusion

A PCB 3D printed scaffold was successfully prepared in this study. Our *in vitro* experiments demonstrated that the scaffold had good biocompatibility, and the addition of BMP-2/PLGA microspheres could markedly improve its *in vitro* bone-enabling ability. These findings provide a new idea for the treatment of long bone shaft and metaphysis defects. So we can also expect that the PCB scaffold will have a broad prospect in the treatment of long bone shaft and metaphysis defects due to its excellent characteristics of easy availability, good biocompatibility, osteogenic properties, and rapid degradation.

Data availability statement

The original contributions presented in the study are included in the article/Supplementary Material, further inquiries can be directed to the corresponding authors.

Ethics statement

Ethical approval was not required for the studies involving humans because the human blood samples were obtained from another researcher (Tao Liu) of our group, whose research has been published on frontier in 2022. The studies were conducted in accordance with the local legislation and institutional requirements.

The human samples used in this study were acquired from primarily isolated as part of your previous study for which ethical approval was obtained. Written informed consent to participate in this study was not required from the participants or the participants' legal guardians/next of kin in accordance with the national legislation and the institutional requirements.

Author contributions

LZ: Writing–original draft, Writing–review and editing, Conceptualization, Data curation, Formal Analysis, Funding acquisition, Investigation, Methodology, Project administration, Resources, Software, Supervision, Validation, Visualization. XZ: Conceptualization, Data curation, Formal Analysis, Funding acquisition, Investigation, Methodology, Project administration, Resources, Software, Supervision, Validation, Visualization, Writing–original draft, Writing–review and editing. FD: Investigation, Software, Conceptualization, Data curation, Formal Analysis, Funding acquisition, Methodology, Project administration, Resources, Supervision, Validation, Visualization, Writing–original draft, Writing–review and editing. XY: Writing–review and editing. YZ: Writing–original draft, Writing–review and editing.

Funding

The author(s) declare that financial support was received for the research, authorship, and/or publication of this article. This work was financially supported by the Guangzhou Science and Technology Program (N0. 201804010136), National Natural Science Foundations of China (grant no. 82360943), the Basic Research Project of Science and Technology Department of Yunnan Province (grant nos 202101AZ070001123, 202201AU070120), Guangdong Basic and Applied Basic Research Foundation (No. 2023A1515110833), China Postdoctoral Science Foundation (No. 2023M740862).

Conflict of interest

The authors declare that the research was conducted in the absence of any commercial or financial relationships that could be construed as a potential conflict of interest.

Publisher's note

All claims expressed in this article are solely those of the authors and do not necessarily represent those of their affiliated organizations, or those of the publisher, the editors and the reviewers. Any product that may be evaluated in this article, or claim that may be made by its manufacturer, is not guaranteed or endorsed by the publisher.

Supplementary material

The Supplementary Material for this article can be found online at: https://www.frontiersin.org/articles/10.3389/fmats.2024.1374409/full#supplementary-material

References

Ahmadian, E., Eftekhari, A., Janas, D., and Vahedi, P. (2023). Nanofiber scaffolds based on extracellular matrix for articular cartilage engineering: a perspective. *Nanotheranostics* 7 (1), 61–69. PMID: 36593799; PMCID: PMC9760364. doi:10.7150/ntno.78611

Chen, D., Zhao, M., and Mundy, G. R. (2004). Bone morphogenetic proteins. *Growth factors.* 22, 233–241. doi:10.1080/08977190412331279890

Chen, S. C., Guo, Y. L., Liu, R. H., Wu, S. Y., Fang, J. H., Huang, B. X., et al. (2018). Tuning surface properties of bone biomaterials to manipulate osteoblastic cell adhesion and the signaling pathways for the enhancement of early osseointegration. *Colloids surfaces. B, Biointerfaces* 164, 58–69. doi:10.1016/j.colsurfb.2018.01.022

Dimitriou, R., Jones, E., McGonagle, D., and Giannoudis, P. V. (2011). Bone regeneration: current concepts and future directions. *BMC Med.* 9, 66. doi:10.1186/1741-7015-9-66

Eugen, G., Claus, M., Anna-Maria, S., Niklas, D., Philipp, S., Andrea, E., et al. (2023). Degradation of 3D-printed magnesium phosphate ceramics *in vitro* and a prognosis on their bone regeneration potential. *Bioact. Mater.* 19, 376–391. doi:10.1016/j.bioactmat.2022.04.015

Farris, A. L., Lambrechts, D., Zhou, Y., Zhang, N. Y., Sarkar, N., Moorer, M. C., et al. (2022). 3D-printed oxygen-releasing scaffolds improve bone regeneration in mice. *Biomaterials* 280, 121318. doi:10.1016/j.biomaterials.2021.121318

Ghorai, S. K., Dutta, A., Roy, T., Guha Ray, P., Ganguly, D., Ashokkumar, M., et al. (2022). Metal ion augmented mussel inspired polydopamine immobilized 3D printed osteoconductive scaffolds for accelerated bone tissue regeneration. *ACS Appl. Mat. Inter.* 14, 28455–28475. doi:10.1021/acsami.2c01657

Giannoudis, P. V., Jones, E., and Einhorn, T. A. (2011). Fracture healing and bone repair. *Injury* 42, 549–550. doi:10.1016/j.injury.2011.03.037

Han, Y., Li, X., Zhang, Y., Han, Y., Chang, F., and Ding, J. (2019). Mesenchymal stem cells for regenerative medicine. *Cells* 8, 886. doi:10.3390/cells8080886

Helaehil, J. V., Lourenco, C. B., Huang, B., Helaehil, L. V., de Camargo, I. X., Chiarotto, G. B., et al. (2021). *In vivo* investigation of polymer-ceramic PCL/HA and PCL/β-TCP 3D composite scaffolds and electrical stimulation for bone regeneration. *Polymers* 14, 65. doi:10.3390/polym14010065

Khalilov, R. (2023). A comprehensive review of advanced nano-biomaterials in regenerative medicine and drug delivery. *Adv. Biol. Ear Sci.* 8 (No.1), 5–18.

Kimura, Y., Miyazaki, N., Hayashi, N., Otsuru, S., Tamai, K., Kaneda, Y., et al. (2010). Controlled release of bone morphogenetic protein-2 enhances recruitment of osteogenic progenitor cells for *de novo* generation of bone tissue. *Part A* 16, 1263–1270. doi:10.1089/ten.TEA.2009.0322

Kumar, G., Tison, C. K., Chatterjee, K., Pine, P. S., McDaniel, J. H., Salit, M. L., et al. (2011). The determination of stem cell fate by 3D scaffold structures through the control of cell shape. *Biomaterials* 32, 9188–9196. doi:10.1016/j.biomaterials.2011.08.054

Kumari, A., Yadav, S. K., and Yadav, S. C. (2010). Biodegradable polymeric nanoparticles based drug delivery systems. *Colloids Surf. B. Biointerfaces* 75, 1–18. doi:10.1016/j.colsurfb.2009.09.001

Lee, H., Yoo, J. J., Kang, H. W., and Cho, D. W. (2016). Investigation of thermal degradation with extrusion-based dispensing modules for 3D bioprinting technology. *Biofabrication* 8, 015011. doi:10.1088/1758-5090/8/1/015011

Lee, S. S., Kim, J. H., Jeong, J., Kim, S. H. L., Koh, R. H., Kim, I., et al. (2020). Sequential growth factor releasing double cryogel system for enhanced bone regeneration. *Biomaterials* 257, 120223. doi:10.1016/j.biomaterials.2020.120223

Li, W., Li, S., Zhang, J., Zhong, H., Liang, J., Huang, S., et al. (2022). Fabrication and evaluation of bone morphogenetic protein-2 microspheres coated black phosphorus nanosheets@polylactic-glycolic acid copolymers scaffold: a multifunctional antibacterial photothermal scaffold for bone regeneration. *Int. J. Biol. Macromol.* 210, 350–364. doi:10.1016/j.ijbiomac.2022.05.028

Liu, J., Sun, L. S., Xu, W. Y., Wang, Q. Q., Yu, S. J., and Sun, J. Z. (2019). Current advances and future perspectives of 3D printing natural-derived biopolymers. *Carbohydr. Polym.* 207, 297–316. doi:10.1016/j.carbpol.2018.11.077

Liu, P., Sun, L., Liu, P., Yu, W., Zhang, Q., Zhang, W., et al. (2018). Surface modification of porous PLGA scaffolds with plasma for preventing dimensional shrinkage and promoting scaffold-cell/tissue interactions. *J. Mater. Chem.* 6, 7605–7613. doi:10.1039/c8tb02374c

Liu, T., Li, Z., Zhao, L., Chen, Z., Lin, Z., Li, B., et al. (2022). Customized design 3D printed PLGA/calcium sulfate scaffold enhances mechanical and biological properties for bone regeneration. *Front. Bioeng. Biotechnol.* 10, 874931. doi:10.3389/fbioe.2022.874931

Lutzweiler, G., Ndreu Halili, A., and Engin Vrana, N. (2020). The overview of porous, bioactive scaffolds as instructive biomaterials for tissue regeneration and their clinical translation. *Pharmaceutics* 12, 602. doi:10.3390/pharmaceutics12070602

Ma, H. S., Feng, C., Chang, J., and Wu, C. T. (2018). 3D-printed bioceramic scaffolds: from bone tissue engineering to tumor therapy. *Acta Biomater.* 79, 37–59. doi:10.1016/j.actbio.2018.08.026

Meijer, G. J., de Bruijn, J. D., Koole, R., and van Blitterswijk, C. A. (2007). Cell-based bone tissue engineering. *PLoS Med.* 4, e9. doi:10.1371/journal.pmed.0040009

Myeroff, C., and Archdeacon, M. (2011). Autogenous bone graft: donor sites and techniques. *J. Bone Jt. Surg. Am.* 93, 2227–2236. doi:10.2106/JBJS.J.01513

Park, J. S., Park, K., Woo, D. G., Yang, H. N., Chung, H. M., and Park, K. H. (2008). PLGA microsphere construct coated with TGF-β 3 loaded nanoparticles for neocartilage formation. *Biomacromolecules* 9, 2162–2169. doi:10.1021/bm800251x

Park, J. Y., Choi, J. C., Shim, J. H., Lee, J. S., Park, H., Kim, S. W., et al. (2014). A comparative study on collagen type I and hyaluronic acid dependent cell behavior for osteochondral tissue bioprinting. *Biofabrication* 6, 035004. doi:10.1088/1758-5082/6/3/035004

Rahmati, M., Silva, E. A., Reseland, J. E., and Haugen, H. J. (2020). Biological responses to physicochemical properties of biomaterial surface. *Chem. Soc. Rev.* 49, 5178–5224. doi:10.1039/d0cs00103a

Sindhura Reddy, N., Sowmya, S., Bumgardner, J. D., Chennazhi, K. P., Biswas, R., and Jayakumar, R. (2014). Tetracycline nanoparticles loaded calcium sulfate composite beads for periodontal management. *Biochim. Biophys. Acta* 1840, 2080–2090. doi:10.1016/j.bbagen.2014.02.007

Sun, J., Zhao, J. H., Bao, X. F., Wang, Q. F., and Yang, X. R. (2018). Alkaline phosphatase assay based on the chromogenic interaction of diethanolamine with 4-aminophenol. *Anal. Chem.* 90, 6339–6345. doi:10.1021/acs.analchem.8b01371

Swanson, W. B., Omi, M., Zhang, Z., Nam, H. K., Jung, Y., Wang, G., et al. (2021). Macropore design of tissue engineering scaffolds regulates mesenchymal stem cell differentiation fate. *Biomaterials* 272, 120769. doi:10.1016/j.biomaterials.2021.120769

Tang, D., Tare, R. S., Yang, L. Y., Williams, D. F., Ou, K. L., and Oreffo, R. O. (2016). Biofabrication of bone tissue: approaches, challenges and translation for bone regeneration. *Biomaterials* 83, 363–382. doi:10.1016/j.biomaterials.2016.01.024

Turnbull, G., Clarke, J., Picard, F., Riches, P., Jia, L. L., Han, F. X., et al. (2018). 3D bioactive composite scaffolds for bone tissue engineering. *Bioact. Mater.* 3, 278–314. doi:10.1016/j.bioactmat.2017.10.001

Wang, C., Huang, W., Zhou, Y., He, L. B., He, Z., Chen, Z. L., et al. (2020). 3D printing of bone tissue engineering scaffolds. *Bioact. Mater.* 5, 82–91. doi:10.1016/j.bioactmat.2020.01.004

Wang, W. S., Cheng, X. H., Liao, J. W., Lin, Z. F., Chen, L. L., Liu, D. D., et al. (2019). Synergistic photothermal and photodynamic therapy for effective implant-related bacterial infection elimination and biofilm disruption using Cu9S8 nanoparticles. *ACS Biomater. Sci. Eng.* 5, 6243–6253. doi:10.1021/acsbiomaterials.9b01280

Wei, G., Jin, Q., Giannobile, W. V., and Ma, P. X. (2006). Nano-fibrous scaffold for controlled delivery of recombinant human PDGF-BB. *J. Control. Release* 112, 103–110. doi:10.1016/j.jconrel.2006.01.011

Xu, X., Sun, M., Wang, D., Bu, W., Wang, Z., Shen, Y., et al. (2019). Bone formation promoted by bone morphogenetic protein-2 plasmid-loaded porous silica nanoparticles with the involvement of autophagy. *Nanoscale* 11, 21953–21963. doi:10.1039/c9nr07017f

Ye, X. L., Zhang, Y. Q., Liu, T., Chen, Z. H., Chen, W. J., Wu, Z. G., et al. (2022). Beta-tricalcium phosphate enhanced mechanical and biological properties of 3D-printed polyhydroxyalkanoates scaffold for bone tissue engineering. *Int. J. Biol. Macromol.* 209, 1553–1561. doi:10.1016/j.ijbiomac.2022.04.056

Zadpoor, A. A. (2019). Meta-biomaterials. *Biomaterials Sci.* 8, 18–38. doi:10.1039/c9bm01247h

Zanotti, S., Smerdel-Ramoya, A., Stadmeyer, L., and Canalis, E. (2008). Activation of the ERK pathway in osteoblastic cells, role of gremlin and BMP-2. *J. Cell. Biochem.* 104, 1421–1426. doi:10.1002/jcb.21715

Zhu, T., Jiang, M., Zhang, M., Cui, L., Yang, X., Wang, X., et al. (2022). Biofunctionalized composite scaffold to potentiate osteoconduction, angiogenesis, and favorable metabolic microenvironment for osteonecrosis therapy. *Bioact. Mater* 9, 446–460. doi:10.1016/j.bioactmat.2021.08.005